Assessment of DLPNO-MP2 Approximations in Double-Hybrid DFT

Hagen Neugebauer,[†] Peter Pinski,[‡] Stefan Grimme,[†] Frank Neese,[*,¶] and Markus Bursch[*,¶]

† *Mulliken Center for Theoretical Chemistry, Clausius Institute for Physical and Theoretical Chemistry, University of Bonn, Beringstr. 4, D-53115 Bonn, Germany*
‡*HQS Quantum Simulations GmbH, Rintheimer Straße 23, D-76131 Karlsruhe, Germany*
¶*Max-Planck-Institut für Kohlenforschung, Kaiser-Wilhelm-Platz 1, D-45470 Mülheim an der Ruhr, Germany*

E-mail: neese@kofo.mpg.de; bursch@kofo.mpg.de

Abstract

The unfavorable scaling (N^5) of conventional second-order Møller-Plesset theory (MP2) typically prevents the application of double-hybrid (DH) density functionals to large systems with more than 100 atoms. A prominent approach to reduce the computational demand of electron correlation methods is the domain-based local pair natural orbital (DLPNO) approximation that is successfully used in the framework of DLPNO-CCSD(T). Its extension to MP2 [P. Pinski, C. Riplinger, E. F. Valeev and F. Neese, *J. Chem. Phys.* **143**, 034108 (2015)] paved the way for DLPNO-MP2-based double-hybrid methods. In this work, we assess the accuracy of the DLPNO-MP2 approximation compared to conventional double-hybrids on a large number of 7925 data points for thermochemistry and 239 data points for structural features including main-group and transition-metal systems. It is shown, that DLPNO-DH-DFT can be applied successfully to perform energy calculations and geometry optimizations for large molecules at a drastically reduces computational cost. Furthermore, PNO space extrapolation is shown to be applicable similar to its DLPNO-CCSD(T) counterpart to reduce the remaining error.

1 Introduction

Kohn-Sham density functional theory (DFT) is widely considered the work-horse of modern computational chemistry. Within the zoo of density functionals available, double-hybrid (DH) functionals typically represent the most accurate approaches.[1–4] The most common double-hybrid functionals employ an admixture of the correlation energy with a fraction a_C computed using second-order perturbation theory (PT2) into the correlation energy expression of the respective density functional (Eq. 1) according to

$$\begin{aligned} E_{XC}^{DH} =&(1-a_X)E_X^{DFT} + a_X E_X^{HF} \\ &+ (1-a_C)E_C^{DFT} + a_C E_C^{PT2}. \end{aligned} \tag{1}$$

One of the first and most prominent double-hybrid functionals is Grimme's B2PLYP functional[5] that employs an 27% ($a_C = 0.27$) admixture of second-order Møller-Plesset perturbation theory (MP2) correlation energy and 53% ($a_X = 0.53$) of "exact" Hartree-Fock exchange.

A critical downside of the MP2-based DH approach is its comparably high computational demand as common MP2 formally scales with $\mathcal{O}(N^5)$ of the system size. Accordingly, approaches to reduce the computational cost of the MP2 part of the DH calculation without losing significant accuracy are desirable. Local wave-function based correlation methods have proven highly successful in this respect. They exploit the spatial locality of electron correlation by truncation of the virtual orbital space thus drastically reducing the number of considered orbitals. The most prominent representative of this class is the domain-based local pair natural orbital (DLPNO) approach that is frequently used in the framework of Coupled-Cluster calculations (e.g. DLPNO-CCSD(T)).[6–9] The DLPNO approach can also be applied to MP2 calculations which renders DLPNO-MP2 a promising candidate to use in the context of double-hybrid DFT.[10] Geometric gradients for closed-shell systems,[11] polarizabilities, and NMR shieldings[12] are also available in a DLPNO-DH scheme.

The efficiency of local methods in the context of DHs has already been demonstrated for main-group thermochemistry for localized pair natural orbitals in combination with F12 explicit correlation by Mehta and Martin.[13] But thorough studies for DLPNO-DHs that investigate the chemical space beyond the GMTKN55 and also consider organometallic compounds are missing. In the following, the DLPNO-MP2 implementation in the ORCA quantum chemistry software package[14,15] is employed for B2PLYP as a representative double-hybrid functional. Its performance is evaluated against the conventional MP2-based B2PLYP functional for a selection of comprehensive bench-

mark sets for thermochemistry and molecule geometries.

2 Methods

2.1 DLPNO Accuracy Settings

Similar to DLPNO-CCSD(T),[16] default accuracy settings for DLPNO-MP2 are available in *ORCA*. These settings are also employed for DLPNO-DH calculations and are shown in Table 1. Albeit *loosePNO* is not meant for accurate DLPNO-MP2 and DLPNO-DH calculations but rather for exploratory calculations, it was tested here because it is available in ORCA via a simple keyword and is relevant in the context of PNO-Space extrapolation. In contrast to DLPNO-CCSD(T), the accuracy thresholds are generally tighter. Additionally, compared to restricted references (RHF/RKS) tighter settings are required for unrestricted calculations (UHF/UKS). Therefore, in benchmark sets involving open-shell systems the tighter thresholds were used for all systems including closed-shell systems.

For a fair assessment of the error introduced by the DLPNO-MP2 approximation, only errors with reference to the conventional MP2-based double-hybrid functional are discussed in the following. This means that no deviations from the original reference data of the investigated benchmark sets are discussed. The error is calculated according to equation 2:

$$\Delta x^{B2PLYP} = x^{B2PLYP}_{DLPNO-MP2} - x^{B2PLYP}_{MP2}. \quad (2)$$

The resulting mean absolute deviation with regard to the conventional DH (MAD_C) is calculated as

$$\mathrm{MAD_C} = \frac{1}{n}\sum_{i}^{n}(\left|\Delta x_i^{B2PLYP}\right|). \quad (3)$$

The MAD_C values are then employed to calculate the WTMAD-2_C according to

$$\mathrm{WTMAD\text{-}2_C} = \frac{56.17\ \mathrm{kcal{\cdot}mol^{-1}}}{\sum_i^{55} N_i}\sum_{i}^{55} N_i \frac{\mathrm{MAD_{C,}}_i}{\overline{|\Delta E|}_i}. \quad (4)$$

Here, 56.17 kcal·mol^{-1}is the the average of the average absolute energies $|\Delta E|_i$ with the reference (B2PLYP) over all 55 sets of the GMTKN55 and N_i is the number of reactions with the $MAD_{C,i}$ for the corresponding set i (See SI for details).

Table 1: PNO key accuracy settings for DLPNO-DHs.

PNO-Settings	T_{CutDO} RKS/UKS	T_{CutPNO} RKS	T_{CutPNO} UKS
loose	$2 \cdot 10^{-2}$	10^{-7}	10^{-8}
normal	$1 \cdot 10^{-2}$	10^{-8}	10^{-9}
tight	$5 \cdot 10^{-3}$	10^{-9}	10^{-10}
verytight	$2.5 \cdot 10^{-3}$	10^{-10}	10^{-11}

2.2 PNO-Space Extrapolation

The computational cost of any DLPNO-MP2 calculation increases drastically upon tightening the T_{CutPNO} threshold. Accordingly, an extrapolation of the PNO space is desirable to obtain high accuracy at reduced computational cost. The extrapolation of the PNO space was successfully applied in the framework of local Coupled-Cluster following Equation 5.[17] Here, E^X and E^Y are the energies (or properties) obtained with the respective T_{CutPNO} thresholds (e.g., $X = 8$ for *normalPNO* with $T_{CutPNO} = 10^{-8}$ and $Y = 9$ for *tightPNO* with $T_{CutPNO} = 10^{-9}$), F is an empirical scaling parameter and E^{XY} is the extrapolated energy:

$$E^{XY} = E^X + F \cdot (E^Y - E^X). \quad (5)$$

Furthermore, it has been shown that the CPS extrapolation reduces the size dependency of the DLPNO error in the context of DLPNO-CCSD(T).[18] In a recent study by Kubas *et al.* a DLPNO-MP2 based extrapolation scheme for DLPNO-CCSD(T) has been proposed.[19] Its good performance suggests that the DLPNO

errors for MP2 and CCSD(T) are rather similar and that CPS extrapolation with a similar F parameter should also be beneficial for DLPNO-MP2. Therefore, in the following, the same F parameter ($F = 1.5$) that has been used for the DLPNO-CCSD(T) CPS extrapolation[17] was assessed for CPS extrapolation in DLPNO-B2PLYP. In this work, $F = 1.5$ proved suitable also for DLPNO-MP2-based DH calculations supporting the findings of Kubas *et al.* In the following the nomenclature for CPS extrapolation will be CPS($X \rightarrow Y$) with l as abbreviation for *loosePNO*, n for *normalPNO*, t for *tightPNO*, and vt for *verytightPNO*.

2.3 Computational Details

All calculations were performed with ORCA version 5.0.4[14,15] employing the B2PLYP double-hybrid functional[5] either with the DLPNO approximation (DLPNO-B2PLYP) or in the conventional form (RI-B2PLYP) in combination with the def2-TZVPP triple-ζ basis[20,21] with the corresponding def2-TZVPP/C auxiliary basis. As integration grid for the DFT calculations the large *DEFGRID3* was employed and for the SCF *TightSCF* settings were selected. Additionally, the Split-RI-J[22] and RIJCOSX[23] approximations were used to speed up the calculations. The frozen core approximation with default settings was used throughout.

3 Results and Discussion

3.1 Thermochemistry

The general main-group thermochemistry, kinetics, and non-covalent interactions (NCIs) database (GMTKN55)[57] was employed to investigate the influence of the DLPNO-MP2 approximation on general main-group thermochemistry. The WTMAD-2_C for different PNO thresholds on the whole GMTKN55 and on the respective subsets with reference to conventional B2PLYP are shown in Table 2. The WTMAD-2_C for the whole GMTKN55 is also depicted in Figure 1.

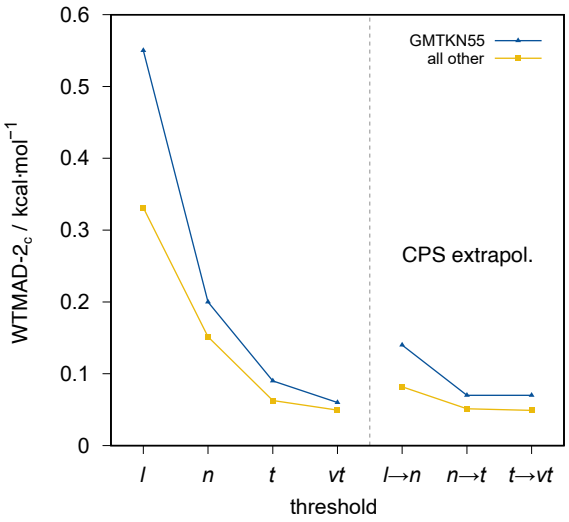

Figure 1: Weighted mean absolute deviations with reference to conventional B2PLYP in kcal·mol^{-1} for the GMTKN55 benchmark set collection and all other thermochemistry benchmark sets assessed (cf. Table 3)

For the whole GMTKN55 database the biggest WTMAD-2_C decrease is observed from *loosePNO* (0.55 kcal·mol^{-1}) to *normalPNO* (0.20 kcal·mol^{-1}) settings and smaller further reductions are obtained with *tightPNO* (0.09 kcal·mol^{-1}) and *verytightPNO* (0.06 kcal·mol^{-1}) settings. In none of the subsets the WTMAD-2_C is above 1 kcal·mol^{-1}except for the intermolecular NCIs when *loosePNO* is employed. For the basic properties subset *loosePNO* only yields a tiny WTMAD-2_C (0.06 kcal·mol^{-1}). Here, only minor improvements in the WTMAD-2_C can be obtained by going up to *verytightPNO* (0.02 kcal·mol^{-1}). This is because the basic property subset mostly contains small molecules. For the reactions subset, the WTMAD-2_C with *loosePNO* is larger (0.47 kcal·mol^{-1}) and still present with *normalPNO* (0.15 kcal·mol^{-1}), but becomes negligible with *tightPNO* (0.07 kcal·mol^{-1}) and *verytightPNO* (0.05 kcal·mol^{-1}) settings. Small errors are also observed for barriers with the WTMAD-2_C for *loosePNO* being already tiny (0.10 kcal·mol^{-1}) with small improvements with *normalPNO* (0.04 kcal·mol^{-1}), but no further improvements with even tighter settings. Larger deviations are observed for the

Table 2: WTMAD-2_C of DLPNO-MP2-based B2PLYP on the GMTKN55 database in kcal·mol^{-1}.

Set	#	*loose*	*normal*	*tight*	*verytight*	CPS(l→n)	CPS(n→t)	CPS(t→vt)
basic	473	0.06	0.03	0.02	0.02	0.03	0.02	0.02
reactions	243	0.47	0.15	0.07	0.05	0.09	0.05	0.04
barriers	194	0.10	0.04	0.04	0.05	0.05	0.05	0.05
inter NCIs	304	1.28	0.47	0.21	0.13	0.25	0.15	0.14
intra. NCIs	291	0.95	0.32	0.15	0.08	0.30	0.11	0.09
GMTKN55	1505	0.55	0.20	0.09	0.06	0.14	0.07	0.07

Table 3: Benchmark sets included in the assessment of DLPNO-B2PLYP with the respective MAD_C in kcal·mol^{-1}. PNO settings are abbreviated (l, n, t, vt). $\overline{|E_{ref.}|}$ is the original mean absolute reference energy of the respective benchmark sets.

Set	#	$\overline{\lvert E_{ref.}\rvert}$	l	n	t	vt	CPS(l→n)	CPS(n→t)	CPS(t→vt)
IONPI19[24]	19	20.87	0.23	0.10	0.04	0.02	0.04	0.02	0.01
R160x6[25,26]	960	2.04	0.02	0.01	0.00	0.00	0.01	0.00	0.00
X40x10[27,28]	400	2.73	0.05	0.02	0.01	0.00	0.01	0.01	0.00
CHAL336[29]	336	14.09	0.12	0.05	0.02	0.01	0.02	0.01	0.01
ACONF-L[30]	50	4.62	0.21	0.08	0.04	0.02	0.03	0.01	0.01
HB300SPX[31]	3000	3.18	0.04	0.02	0.01	0.01	0.01	0.01	0.01
revBH9$_{BH}$[32,33]	898	20.37	0.31	0.12	0.05	0.04	0.05	0.02	0.04
revBH9$_{RE}$[32,33]	449	11.08	0.19	0.08	0.03	0.02	0.04	0.02	0.03
LP14[34]	14	23.33	1.04	0.48	0.23	0.10	0.21	0.11	0.04
L7[35,36]	7	16.27	1.34	0.60	0.24	0.08	0.23	0.08	0.02
S30L[37]	30	37.51	2.52	1.22	0.60	0.26	0.57	0.28	0.10
HS13L[a 38]	13	45.82	2.29	1.14	0.57	0.28	0.57	0.29	0.13
MOR41[39]	41	31.20	0.60	0.26	0.11	0.05	0.10	0.04	0.02
ROST61[40]	61	42.78	0.40	0.18	0.09	0.05	0.08	0.05	0.03
WCCR10[41,42]	10	48.72	1.12	0.51	0.22	0.09	0.21	0.10	0.04
TMCONF16[43]	16	3.15	0.04	0.02	0.01	0.00	0.03	0.01	0.00
TMBH[44–47]	40	14.47	0.14	0.05	0.02	0.01	0.02	0.01	0.01
MOBH35[48–50]	70	20.89	0.25	0.09	0.04	0.02	0.04	0.02	0.01
TMIP[51]	11	95.62	0.58	0.28	0.13	0.06	0.14	0.06	0.03

Table 4: Geometry benchmark sets included in the assessment of DLPNO-B2PLYP/TZ. Mean absolute deviations (MAD_C), and mean deviations (MD_C) in pm, °, or MHz. All deviations are given relative to the conventional MP2-based double-hybrid functional. $\overline{|x_{ref.}|}$ is the original mean absolute reference structural property of the respective benchmark sets.

			loose		*normal*		*tight*		*verytight*	
Set	#	$\overline{\lvert x_{ref.}\rvert}$	MAD_C	MD_C	MAD_C	MD_C	MAD_C	MD_C	MAD_C	MD_C
$CCse21_{bonds}$ [52,53]	68	122.33	0.003	0.001	0.002	0.001	0.002	0.000	0.002	0.000
$CCse21_{angles}$ [52,53] [°]	42	116.03	0.004	0.000	0.004	0.000	0.004	0.000	0.004	0.000
ROT34[a] [54] [MHz]	34	1411.72	0.526	−0.379	0.224	−0.129	0.051	−0.050	0.013	−0.009
HMGB11 [55]	11	243.40	0.055	0.055	0.019	0.019	0.006	0.006	0.004	0.001
LMGB35[a] [55]	26	114.01	0.003	0.000	0.003	0.000	0.003	0.000	0.003	0.000
LB12 [55]	12	299.26	0.701	0.689	0.339	0.323	0.164	0.152	0.083	0.059
TMC32[a,b] [56]	46	189.47	0.298	0.047	0.070	0.033	0.035	0.020	0.024	0.015

[a] Open-shell systems were excluded as no gradient is yet available for them. [b] $Fe(CO)_2(NO)_2$ was excluded due to convergence problems with B2PLYP.

inter and intramolecular NCI subsets where *loosePNO* yields WTMAD-2_C values around 1 kcal·mol^{-1}. These WTMAD-2_C values are reduced to a third by employing *normalPNO* (0.47 kcal·mol^{-1}and 0.32 kcal·mol^{-1}) and further halved by using *tightPNO* (0.21 kcal·mol^{-1}and 0.15 kcal·mol^{-1}) and *verytightPNO* (0.13 kcal·mol^{-1}and 0.08 kcal·mol^{-1}) settings. The CPS extrapolation general reduces the WTMAD-2_C for CPS(l→n) and CPS(n→t) but no improvement is observed for CPS(t→vt). Since the errors with *tightPNO* are almost converged with regard to the PNO thresholds, no further improvement is obtained by CPS(t→vt) extrapolation in this case. The improvement from *normalPNO* to CPS(l→n) is larger (from 0.20 kcal·mol^{-1}to 0.14 kcal·mol^{-1}) than from *tightPNO* to CPS(n→t) (from 0.09 kcal·mol^{-1}to 0.07 kcal·mol^{-1}). For the GMTKN55 *tightPNO* and tighter settings and CPS(n→t) and higher can be considered as converged, because WTMAD-2_C values smaller than 0.1 kcal·mol^{-1}are obtained. Such errors are negligible for practical applications in comparison to the overall DH errors.

In addition to the GMTKN55, several benchmark sets were considered. The results are shown in Table 3 and an overall weighted MAD_C in Figure 1. These include sets for NCIs of large systems (L7,[35,36] S30L,[37] and HS13L[38]), ion-π interactions (IONPI19[24]), halogen bonds (X40x10[27,28]), hydrogen bonds (HB300SPX[31]), chalcogen bonds (CHAL336[29]), frustrated Lewis pairs (LP14), conformational energies of alkanes (ACONF-L[30]), and repulsive NCIs (R160x6[25]). For barrier heights and reaction energies, the revBH9[32,33] set is included. Also included are sets containing transition metal complexes for closed-shell reaction energies (MOR41[39] and WCCR10[41,42]), open-shell reaction energies (ROST61[40]), conformational energies (TMCONF16[43]), barrier heights (MOBH35[48,49] and TMBH[44–47]), and ionization energies (TMIP[51]).

The largest errors are obtained for the NCI sets containing large systems. For the S30L *loosePNO* yields an MAD_C of 2.52 kcal·mol^{-1}that is larger than the MAD_Cs of the best performing DFT methods for this set (around 2 kcal·mol^{-1}). Tightening the PNO settings successively halves the MAD_C for this set from *normalPNO* (1.22 kcal·mol^{-1}) to *tightPNO* (0.60 kcal·mol^{-1}) to *verytightPNO* (0.26 kcal·mol^{-1}). Here, CPS(t→vt) yields a basically converged MAD_C of 0.10 kcal·mol^{-1}, but due to the many $\pi-\pi$ interactions in the S30L (as for the HS13L, L7, and LP14) the application of double-hybrid functionals to this set is questionable in the first place. Similar behav-

ior as for the S30L is observed for the HS13L. Less prone but still severe are the MAD_Cs of the L7 and the LP14 sets where the MAD_Cs (as the average interaction energies) are basically halved compared to the S30L and HS13L. Much smaller are the MAD_Cs for the IONPI19, the revBH9, and the ACONF-L set where MAD_Cs of 0.1 kcal·mol^{-1}are already reached with *normalPNO* except for the barriers of the revBH9 by 0.02 kcal·mol^{-1}. The MAD_Cs of the CHAL336, X40x10, HB300SPX, and the R160x6 sets are already small with *loosePNO* and become vanishing small with tighter settings. This may again be attributed to the relatively small system size of the molecules in these sets. For the transition metal containing sets the WCCR10 shows the largest MAD_Cs (1.12 kcal·mol^{-1}with *loosePNO*) followed by the MOR41, the TMIP, and the ROST61 (between 0.4-0.6 kcal·mol^{-1}with *loosePNO*). Smaller errors are observed for the MOBH35 and the TMBH, where all settings tighter than *loosePNO* yield MAD_Cs smaller than 0.1 kcal·mol^{-1}. Surprising are the vanishing MAD_Cs for the TMCONF16 set. In conclusion, the errors for the organometallic sets are larger than for typical organic reactions but with *tightPNO* settings or CPS($l \rightarrow n$) the MAD_Cs are around 0.1 kcal·mol^{-1}(with one exception). This error is negligible compared to the errors of the corresponding double-hybrid. Finally, as a good compromise between computational cost and accuracy, we recommend employing *normalPNO* for the gradient calculation of medium-sized organic compounds (up to 100 atoms) and conventional MP2-DHs for the energy evaluation as the latter does not profit from the DLPNO approximation speedup. In the regime of 100 atoms and larger, DLPNO-MP2-DHs yield increasing speedup and may be employed with *normalPNO* for most systems. In this context, the DLPNO approximation starts to generally enable DH calculations that would be unfeasible for such large systems due to computation time and memory issues. In terms of PNO-space extrapolation, we recommend CPS($l \rightarrow n$) for reaction and CPS($n \rightarrow t$) for non-covalent interactions.

3.2 Varying MP2 Contribution

As double-hybrid functionals typically include different amounts of MP2 correlation in their energy expression (cf. Equation 1) the estimated error introduced by the DLPNO-MP2 approximation can vary as well. Nevertheless, the introduced error behaves linearly with the amount of MP2 correlation which is demonstrated for DLPNO-B2PLYP variants with varying amounts of MP2 of 20, 40, 60, and 80% on the L7 set (Figure 2). Accordingly,

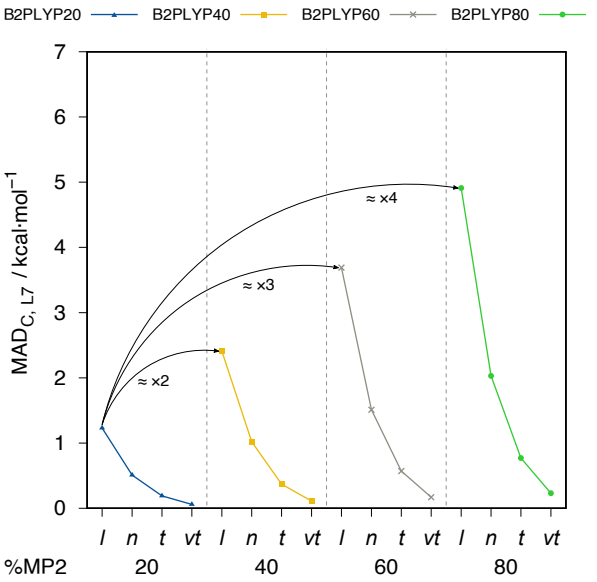

Figure 2: MAD_Cs for the L7 benchmark set for B2PLYP variants with varying amounts of MP2 correlation with reference to conventional B2PLYP in kcal·mol^{-1}. l = *loosePNO*, n = *normalPNO*, t = *tightPNO*, vt = *verytightPNO*.

tripling the amount of MP2 correlation triples the DLPNO-MP2 error with respect to conventional B2PLYP. Nevertheless, most robust and well-behaved double-hybrids employ values of around 30% MP2 correlation, allowing for a reasonable error estimate based on the results for B2PLYP (27% MP2).

3.3 Size dependence of correlation energy error

In line with previous findings on PNO errors in DLPNO-CCSD(T) approaches, the correlation energy error with respect to conventional

B2PLYP behaves almost linearly with the size of the system. This is demonstrated for a polyalanine chain (Figure 3) where a clear decrease in the size dependence upon tightening the PNO thresholds is observed. Further, even a CPS($l \rightarrow n$) PNO space extrapolation can eliminate most of the size-dependent correlation energy error for this case.

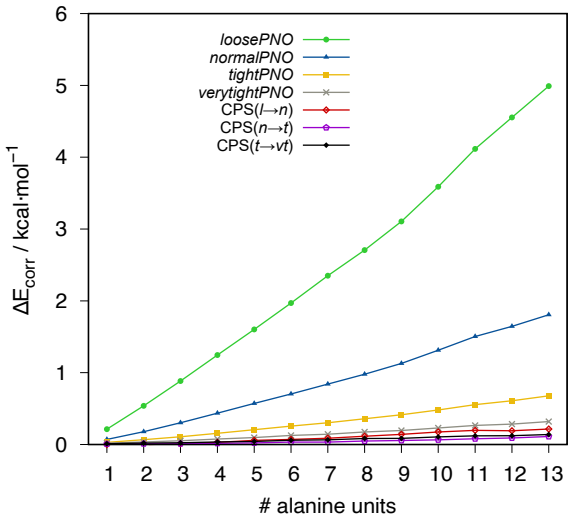

Figure 3: Error in MP2 correlation energy with reference to conventional B2PLYP in kcal·mol^{-1} for polyalanines.

3.4 Geometry Optimizations

As even energy calculations on a high theoretical level such as double-hybrid DFT are computationally demanding, geometry optimizations requiring many energy and gradient evaluations are typically unfeasible. Nevertheless, highly accurate geometry optimizations are desirable for critical cases and specifically benchmarking more approximate methods such as semi-empirical quantum mechanics (SQM) or force-fields (FF). By employing DLPNO-MP2, respective double-hybrid functionals become feasible again for geometry optimizations of medium-sized to large molecules. To estimate the influence of the DLPNO-MP2 threshold settings, DLPNO-B2PLYP geometry optimizations were performed for various established geometry optimization benchmark sets. The resulting geometries were compared to the conventional MP2-based B2PLYP results (Figure 4 and Table 4). The following geometric features were investigated: Rotational constants for small to medium-sized organic molecules were compared (ROT34.[54] Bond lengths were compared for 3d transition metal complexes (TMC32[56]) and light (LMGB35[55]) and heavy (HMGB11[55]) main-group compounds as well as a mixed set containing unusually long bonds (LB12[55]). Additionally, for the CCe21 set,[52,53] containing semi-experimental structures of organic molecules, bond distances and angles were compared. No effect of the accuracy settings is observed for the LMGB35 and the conventional B2PLYP bond lengths are almost obtained with a vanishing MAD_C of 0.003 pm because the molecules in this test set are very small. Similar errors are observed for the CCse21 and

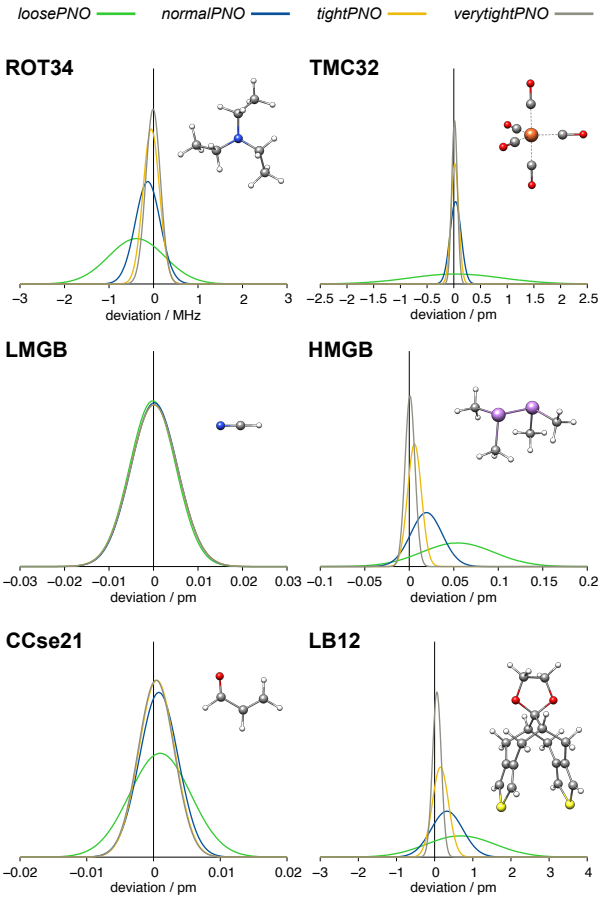

Figure 4: Gaussian error distributions for selected bond length benchmark sets with reference to conventional B2PLYP results. Negative mean deviations indicate overall too short bond lengths compared to the canocial result.

the HMGB11 set. Although here small differences between the PNO settings are observed. Larger errors that are still below 1 pm are found for the TMC32 and the LB12 set with *loosePNO*. For the TMC32 *normalPNO* is already sufficient, while for the LB12 set errors below 0.1 pm are only obtained with *verytightPNO*. For the ROT34 small MAD_Cs are observed with *loosePNO* (0.526 MHz) and *normalPNO* (0.224 MHz) and basically vanish with *tightPNO* (0.051 MHz). In general, the introduced errors of the DLPNO approximation are very small compared to the B2PLYP result. In all cases MAD_Cs below 1 pm, 1 MHz, or 1 [°] were obtained. The very small differences between the structures obtained using varying PNO thresholds and conventional B2PLYP can also be seen for the large frustrated Lewis-pair (FLP) system of the LB12 benchmark set. An overlay of all optimized structures shows no significant difference in the optimized structures (Figure 5), underlining the value of using less tight PNO thresholds for geometry optimizations. Overall, the errors introduced by

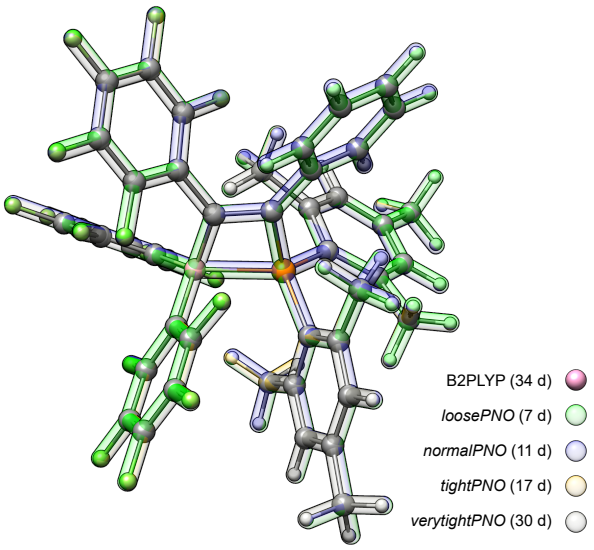

Figure 5: Structure overlay of the FLP (88 atoms) from the LB12 benchmark set optimized at various PNO threshold settings. All optimizations were performed on 4 CPUs using an Intel® Xeon® CPU E3-1270 v5 @ 3.60GHz machine.

the DLPNO-MP2 approximation are generally much less pronounced for geometrical features. This renders the efficient *normalPNO* settings already suitable for DLPNO-DH geometry optimizations of large systems.

3.5 Timing Comparisons

The computational demand of energy and gradient evaluations typically determines the feasibility of a geometry optimization. Therefore, the computational wall-time reduction of a subsequent energy and gradient calculation is assessed for various PNO thresholds for polyalanine with varying chain length (Figure 6).

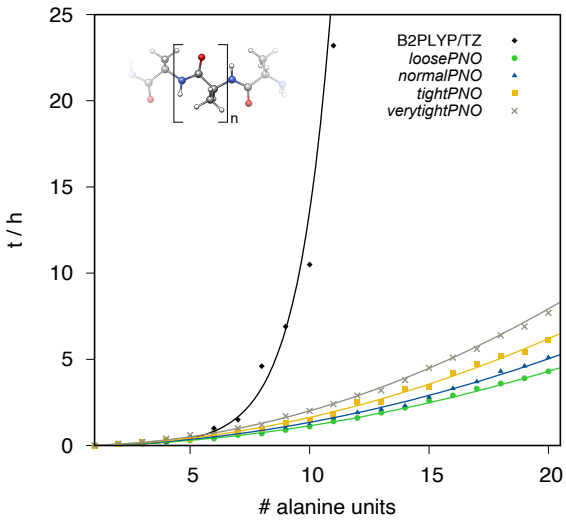

Figure 6: Computation wall-times in h for energy and gradient evaluation of polyalanine chains with up to 20 alanine units (203 atoms) for conventional B2PLYP/def2-TZVP and DLPNO-B2PLYP/def2-TZVP with different PNO thresholds. All calculations were performed on 14 CPUs using an Intel® Xeon® CPU E5-2660 v4 @ 2.00GHz machine.

At a crossing point of about five alanine units (53 atoms), the DLPNO-MP2 approximation begins to drastically reduce the computation time of the combined energy and gradient compared to conventional MP2. The steep scaling of the latter causes a drastic increase in computation time while the DLPNO-MP2-based approach yields a flat, almost linear, scaling with the size of the system. A comparison of the energy and gradient computation time contributions for the parental hybrid functional and

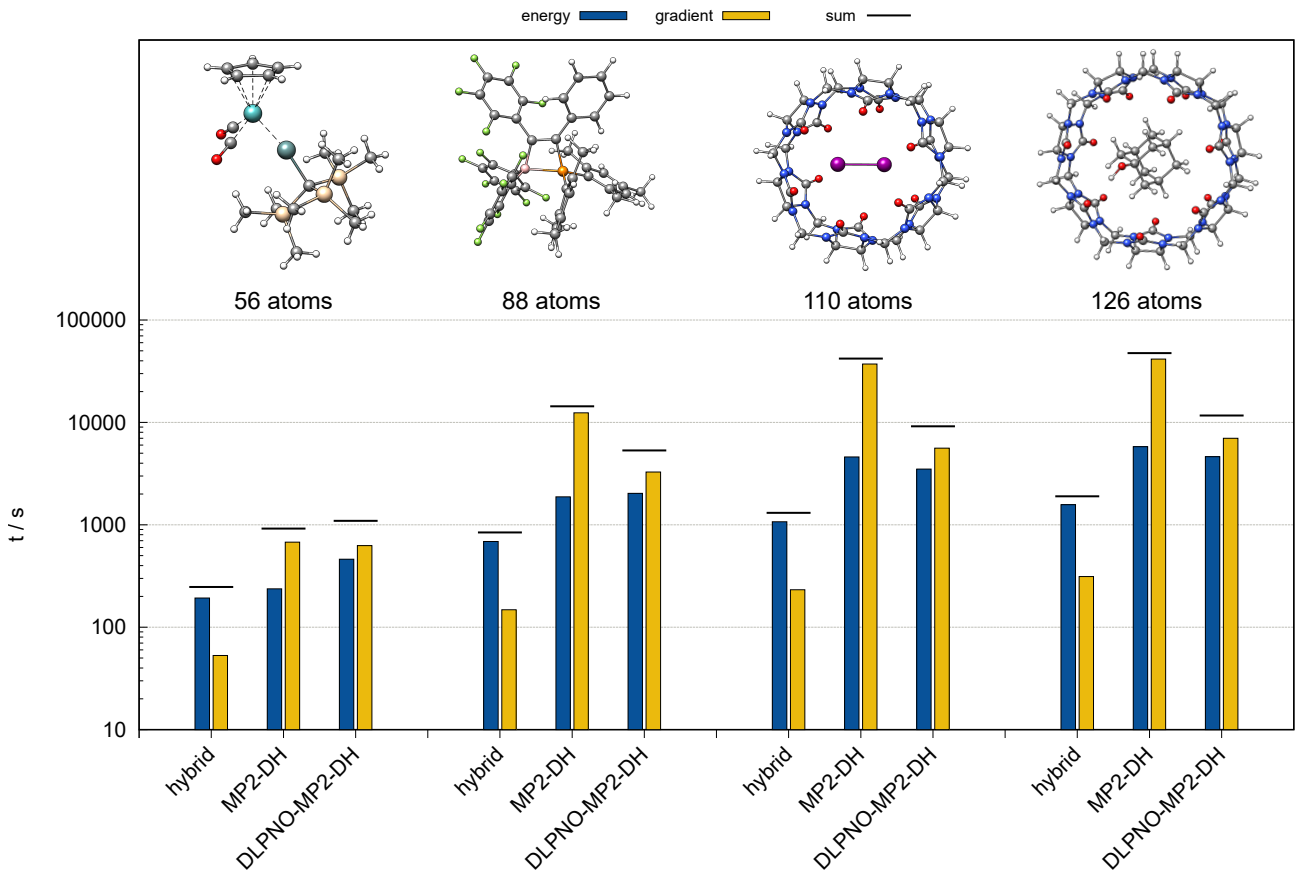

Figure 7: Computation times in s for energy and gradient evaluation of selected molecules in the range of 56 to 126 atoms. Hybrid = BLYP with 53% HFX; MP2-DH = B2PLYP; DLPNO-MP2-DH = DLPNO-B2PLYP with *normalPNO* thresholds. The def2-TZVP(-f) basis was used throughout. All calculations were performed on 14 CPUs using an Intel® Xeon® CPU E5-2660 v4 @ 2.00GHz machine. Note the logarithmic scale.

the double-hybrid variants is depicted in figure 7. In line with the results shown for the polyalanine chain, the gradient evaluation profits significantly from the DLPNO-MP2 approximation, even for medium sized molecules such as the depicted molybdosilylidine complex with 56 atoms. Nevertheless, for these molecule sizes the overhead of the DLPNO space construction causes more costly energy evaluations compared to conventional MP2, thus resulting in a higher overall computation time. With increasing size, the energy computation using the DLPNO approximation becomes increasingly faster, and the benefit for the gradient evaluation is even more drastic underlining the value of DLPNO-MP2-DH calculations for molecules with more than 100 atoms.

4 Conclusion

In this work, the application of the DLPNO-MP2 approximation in the double-hybrid DFT framework was assessed. The performance of different PNO thresholds as well as PNO space extrapolations was tested for the prominent B2PLYP functional on various benchmark sets for the thermochemistry of main-group molecules and transition metal complexes. It was demonstrated that *tightPNO* settings yield reliably small deviations from conventional B2PLYP at a drastically reduced computational cost for large systems (WTMAD-2_C^{all}=0.06 kcal·mol^{-1}, WTMAD-$2_C^{GMTKN55}$=0.09 kcal·mol^{-1}).

In general we expect that the observed DLPNO error is transferable to other double-hybrid functionals as the error behaves lin-

early with the amount of the MP2 correlation admixture. The errors for geometry optimizations were found to be even smaller and in many cases negligibly small even at moderately tight PNO thresholds. *normalPNO* yields already satisfactory agreement with geometries optimized with conventional B2PLYP. The CPS extrapolation scheme introduced in the DLPNO-CCSD(T) framework was successfully applied to DLPNO-MP2-based double hybrid calculations, with CPS($n \rightarrow t$) typically yielding accurate results with very small residual errors compared to the conventional double hybrid (WTMAD-2_C^{all}=0.05 kcal·mol^{-1}, WTMAD-$2_C^{GMTKN55}$=0.07 kcal·mol^{-1}). The CPS parameter $F = 1.5$ was found to be also suitable in the DLPNO-DH-DFT framework.

The performance of DLPNO-DH-DFT can potentially also benefit from employing the so-called tightened semicore settings as proposed by Altun*et al.*[58] for transition metal complexes or modified PNO settings as proposed by Werner and Hansen.[59]

Overall, it is demonstrated that DLPNO-DH-DFT represents a valuable alternative to conventional DH-DFT for large systems where the unfavorable N^5 scaling of MP2 prevents its application. DLPNO-DH-DFT may be applied to enable highly accurate geometry optimizations and energy calculations of large molecules that are unfeasible with conventional double-hybrid functionals. Further, the technical implementation of DLPNO-MP2 is much easier compared to its DLPNO-CCSD(T) counterpart, increasing its potential availability in common quantum chemistry programs.

Supporting Information Available

See the supplementary material for statistical data.

Acknowledgement The German Science Foundation (DFG) is gratefully acknowledged for financial support (Grant 1927/16-1). Further, SG and MB gratefully acknowledge financial support of the Max Planck Society through the Max Planck fellow program.

References

(1) Goerigk, L.; Grimme, S. Double-hybrid density functionals. *WIREs Comput. Mol. Sci.* **2014**, *4*, 576–600.

(2) Mehta, N.; Casanova-Páez, M.; Goerigk, L. Semi-empirical or non-empirical double-hybrid density functionals: which are more robust? *Phys. Chem. Chem. Phys.* **2018**, *20*, 23175–23194.

(3) Martin, J. M. L.; Santra, G. Empirical Double-Hybrid Density Functional Theory: A 'Third Way' in Between WFT and DFT. *Isr. J. Chem.* **2020**, *60*, 787–804.

(4) Bursch, M.; Mewes, J.-M.; Hansen, A.; Grimme, S. Best-Practice DFT Protocols for Basic Molecular Computational Chemistry. *Angew Chem. Int. Ed.* **2022**, *61*, e202205735.

(5) Grimme, S. Semiempirical hybrid density functional with perturbative second-order correlation. *J. Chem. Phys.* **2006**, *124*, 034108.

(6) Riplinger, C.; Sandhoefer, B.; Hansen, A.; Neese, F. Natural triple excitations in local coupled cluster calculations with pair natural orbitals. *J. Chem. Phys.* **2013**, *139*, 134101.

(7) Hansen, A.; Liakos, D. G.; Neese, F. Efficient and accurate local single reference correlation methods for high-spin open-shell molecules using pair natural orbitals. *J. Chem. Phys.* **2011**, *135*, 214102.

(8) Saitow, M.; Becker, U.; Riplinger, C.; Valeev, E. F.; Neese, F. A new near-linear scaling, efficient and accurate, open-shell domain-based local pair natural orbital coupled cluster singles and doubles theory. *J. Chem. Phys.* **2017**, *146*, 164105.

(9) Riplinger, C.; Pinski, P.; Becker, U.; Valeev, E. F.; Neese, F. Sparse maps—A

systematic infrastructure for reduced-scaling electronic structure methods. II. Linear scaling domain based pair natural orbital coupled cluster theory. *J. Chem. Phys.* **2016**, *144*, 024109.

(10) Pinski, P.; Riplinger, C.; Valeev, E. F.; Neese, F. Sparse maps—A systematic infrastructure for reduced-scaling electronic structure methods. I. An efficient and simple linear scaling local MP2 method that uses an intermediate basis of pair natural orbitals. *J. Chem. Phys.* **2015**, *143*, 034108.

(11) Pinski, P.; Neese, F. Analytical gradient for the domain-based local pair natural orbital second order Møller-Plesset perturbation theory method (DLPNO-MP2). *J. Chem. Phys.* **2019**, *150*, 164102.

(12) Stoychev, G. L.; Auer, A. A.; Gauss, J.; Neese, F. DLPNO-MP2 second derivatives for the computation of polarizabilities and NMR shieldings. *J. Chem. Phys.* **2021**, *154*, 164110.

(13) Mehta, N.; Martin, J. M. L. Reduced-Scaling Double Hybrid Density Functional Theory with Rapid Basis Set Convergence through Localized Pair Natural Orbital F12. *J. Phys. Chem. Lett.* **2022**, *13*, 9332–9338, PMID: 36178852.

(14) ORCA – an ab initio, density functional and semiempirical program package, V. 5.0.4, F. Neese, MPI für Kohlenforschung, Mülheim a. d. Ruhr (Germany), **2023**.

(15) Neese, F. Software update: The ORCA program system—Version 5.0. *Wiley Interdiscip. Rev. Comput. Mol. Sci.* **2022**, e1606.

(16) Liakos, D. G.; Sparta, M.; Kesharwani, M. K.; Martin, J. M. L.; Neese, F. Exploring the Accuracy Limits of Local Pair Natural Orbital Coupled-Cluster Theory. *J. Chem. Theory Comput.* **2015**, *11*, 1525–1539, PMID: 26889511.

(17) Altun, A.; Neese, F.; Bistoni, G. Extrapolation to the Limit of a Complete Pair Natural Orbital Space in Local Coupled-Cluster Calculations. *J. Chem. Theory Comput.* **2020**, *16*, 6142–6149, PMID: 32897712.

(18) Altun, A.; Ghosh, S.; Riplinger, C.; Neese, F.; Bistoni, G. Addressing the System-Size Dependence of the Local Approximation Error in Coupled-Cluster Calculations. *J. Phys. Chem. A* **2021**, *125*, 9932–9939, PMID: 34730360.

(19) Pogrebetsky, J.; Siklitskaya, A.; Kubas, A. MP2-Based Correction Scheme to Approach the Limit of a Complete Pair Natural Orbitals Space in DLPNO-CCSD(T) Calculations. *J. Chem. Theory Comput.* **0**, *0*, null, PMID: 37338422.

(20) Weigend, F.; Ahlrichs, R. Balanced basis sets of split valence, triple zeta valence and quadruple zeta valence quality for H to Rn: Design and assessment of accuracy. *Phys. Chem. Chem. Phys.* **2005**, *7*, 3297–3305.

(21) Weigend, F. Accurate Coulomb-fitting basis sets for H to Rn. *Phys. Chem. Chem. Phys.* **2006**, *8*, 1057–1065.

(22) Neese, F. An improvement of the resolution of the identity approximation for the formation of the Coulomb matrix. *J. Comput. Chem.* **2003**, *24*, 1740–1747.

(23) Helmich-Paris, B.; de Souza, B.; Neese, F.; Izsák, R. An improved chain of spheres for exchange algorithm. *J. Chem. Phys.* **2021**, *155*, 104109.

(24) Spicher, S.; Caldeweyher, E.; Hansen, A.; Grimme, S. Benchmarking London dispersion corrected density functional theory for noncovalent ion-π interactions. *Phys. Chem. Chem. Phys.* **2021**, *23*, 11635–11648.

(25) Miriyala, V. M.; Řezáč, J. Testing Semiempirical Quantum Mechanical Methods on a Data Set of Interaction

Energies Mapping Repulsive Contacts in Organic Molecules. *J. Phys. Chem. A* **2018**, *122*, 2801–2808.

(26) Miriyala, V. M.; Řezáč, J. Correction to: Testing semiempirical QM methods on a data set of interaction energies mapping repulsive contacts in organic molecules (Journal of Physical Chemistry A (2018) 122 :10 (2801–2808) DOI: 10.1021/acs.jpca.8b00260). *J. Phys. Chem. A* **2018**, *122*, 9585–9586.

(27) Kesharwani, M. K.; Manna, D.; Sylvetsky, N.; Martin, J. M. L. The X40×10 Halogen Bonding Benchmark Revisited: Surprising Importance of (n-1)d Subvalence Correlation. *J. Phys. Chem. A* **2018**, *122*, 2184–2197.

(28) Kesharwani, M. K.; Manna, D.; Sylvetsky, N.; Martin, J. M. The X40×10 Halogen Bonding Benchmark Revisited: Surprising Importance of (n-1)d Subvalence Correlation. *J. Phys. Chem. A* **2018**, *122*, 2184–2197.

(29) Mehta, N.; Fellowes, T.; White, J. M.; Goerigk, L. CHAL336 Benchmark Set: How Well Do Quantum-Chemical Methods Describe Chalcogen-Bonding Interactions? *J. Chem. Theory Comput.* **2021**, *17*, 2783–2806.

(30) Ehlert, S.; Grimme, S.; Hansen, A. Conformational Energy Benchmark for Longer n-Alkane Chains. *J. Phys. Chem. A* **2022**, *126*, 3521–3535.

(31) Řezáč, J. Non-Covalent Interactions Atlas Benchmark Data Sets 2: Hydrogen Bonding in an Extended Chemical Space. *J. Chem. Theory Comput.* **2020**, *16*, 6305–6316.

(32) Prasad, V. K.; Pei, Z.; Edelmann, S.; Otero-De-La-Roza, A.; Dilabio, G. A. BH9, a New Comprehensive Benchmark Data Set for Barrier Heights and Reaction Energies: Assessment of Density Functional Approximations and Basis Set Incompleteness Potentials. *J. Chem. Theory Comput.* **2022**, *18*, 151–166.

(33) Prasad, V. K.; Pei, Z.; Edelmann, S.; Otero-De-La-Roza, A.; Dilabio, G. A. Correction: BH9, a new comprehensive benchmark data set for barrier heights and reaction energies: Assessment of density functional approximations and basis set incompleteness potentials (J. Chem. Theory Comput. (2022) 18:1 (151-166) DO. 2022; `https://pubs.acs.org/doi/full/10.1021/acs.jctc.2c00362`.

(34) Bistoni, G.; Auer, A. A.; Neese, F. Understanding the Role of Dispersion in Frustrated Lewis Pairs and Classical Lewis Adducts: A Domain-Based Local Pair Natural Orbital Coupled Cluster Study. *Chem. - A Eur. J.* **2017**, *23*, 865–873.

(35) Sedlak, R.; Janowski, T.; Pitoňák, M.; Řezáč, J.; Pulay, P.; Hobza, P. Accuracy of quantum chemical methods for large noncovalent complexes. *J. Chem. Theory Comput.* **2013**, *9*, 3364–3374.

(36) Al-Hamdani, Y. S.; Nagy, P. R.; Zen, A.; Barton, D.; Kállay, M.; Brandenburg, J. G.; Tkatchenko, A. Interactions between large molecules pose a puzzle for reference quantum mechanical methods. *Nat. Commun.* **2021**, *12*, 1–12.

(37) Sure, R.; Grimme, S. Comprehensive Benchmark of Association (Free) Energies of Realistic Host–Guest Complexes. *J. Chem. Theory Comput.* **2015**, *11*, 3785–3801.

(38) Gorges, J.; Grimme, S.; Hansen, A. Reliable prediction of association (free) energies of supramolecular complexes with heavy main group elements - the HS13L benchmark set. *Phys. Chem. Chem. Phys.* **2022**, *24*, 28831–28843.

(39) Dohm, S.; Hansen, A.; Steinmetz, M.; Grimme, S.; Checinski, M. P. Comprehensive Thermochemical Benchmark Set of

Realistic Closed-Shell Metal Organic Reactions. *J. Chem. Theory Comput* **2018**, *14*, 2596–2608.

(40) Maurer, L. R.; Bursch, M.; Grimme, S.; Hansen, A. Assessing Density Functional Theory for Chemically Relevant Open-Shell Transition Metal Reactions. *J. Chem. Theory Comput* **2021**, *17*, 6134–6151.

(41) Husch, T.; Freitag, L.; Reiher, M. Calculation of Ligand Dissociation Energies in Large Transition-Metal Complexes. *J. Chem. Theory Comput.* **2018**, *14*, 2456–2468.

(42) Husch, T.; Freitag, L.; Reiher, M. Correction to: 'Calculation of ligand dissociation energies in large transition-metal complexes' (J. Chem. Theory Comput. (2018) 14:5 (2456–2468) DOI: 10.1021/acs.jctc.8b00061). *J. Chem. Theory Comput.* **2019**, *15*, 4295–4296.

(43) Bursch, M.; Hansen, A.; Pracht, P.; Kohn, J. T.; Grimme, S. Theoretical study on conformational energies of transition metal complexes. *Phys. Chem. Chem. Phys.* **2021**, *23*, 287–299.

(44) Sun, Y.; Chen, H. Performance of Density Functionals for Activation Energies of Re-Catalyzed Organic Reactions. *J. Chem. Theory Comput.* **2014**, *10*, 579–588.

(45) Sun, Y.; Chen, H. Performance of density functionals for activation energies of Zr-mediated reactions. *J. Chem. Theory Comput.* **2013**, *9*, 4735–4743.

(46) Sun, Y.; Hu, L.; Chen, H. Comparative Assessment of DFT Performances in Ru- and Rh-Promoted σ-Bond Activations. *J. Chem. Theory Comput* **2015**, *11*, 1428–1438.

(47) Hu, L.; Chen, H. Assessment of DFT Methods for Computing Activation Energies of Mo/W-Mediated Reactions. *J. Chem. Theory Comput.* **2015**, *11*, 4601–4614.

(48) Iron, M. A.; Janes, T. Evaluating Transition Metal Barrier Heights with the Latest Density Functional Theory Exchange-Correlation Functionals: The MOBH35 Benchmark Database. *J. Phys. Chem. A* **2019**, *123*, 3761–3781.

(49) Iron, M. A.; Janes, T. Correction to 'Evaluating Transition Metal Barrier Heights with the Latest Density Functional Theory Exchange-Correlation Functionals: The MOBH35 Benchmark Database'. *J. Phys. Chem. A* **2019**, *123*, 3761–3781.

(50) Dohm, S.; Bursch, M.; Hansen, A.; Grimme, S. Semiautomated Transition State Localization for Organometallic Complexes with Semiempirical Quantum Chemical Methods. *J. Chem. Theory Comput.* **2020**, *16*, 2002–2012.

(51) Rudshteyn, B.; Weber, J. L.; Coskun, D.; Devlaminck, P. A.; Zhang, S.; Reichman, D. R.; Shee, J.; Friesner, R. A. Calculation of Metallocene Ionization Potentials via Auxiliary Field Quantum Monte Carlo: Toward Benchmark Quantum Chemistry for Transition Metals. *J. Chem. Theory Comput.* **2021**, *18*, 2845–2862.

(52) Piccardo, M.; Penocchio, E.; Puzzarini, C.; Biczysko, M.; Barone, V. Semi-Experimental Equilibrium Structure Determinations by Employing B3LYP/SNSD Anharmonic Force Fields: Validation and Application to Semirigid Organic Molecules. *J. Phys. Chem. A* **2015**, *119*, 2058–2082.

(53) Brémond, É.; Savarese, M.; Su, N. Q.; Pérez-Jiménez, Á. J.; Xu, X.; Sancho-García, J. C.; Adamo, C. Benchmarking Density Functionals on Structural Parameters of Small-/Medium-Sized Organic Molecules. *J. Chem. Theory Comput.* **2016**, *12*, 459–465.

(54) Risthaus, T.; Steinmetz, M.; Grimme, S. Implementation of nuclear gradients of

range-separated hybrid density functionals and benchmarking on rotational constants for organic molecules. *J. Comput. Chem.* **2014**, *35*, 1509–1516.

(55) Grimme, S.; Brandenburg, J. G.; Bannwarth, C.; Hansen, A. Consistent structures and interactions by density functional theory with small atomic orbital basis sets. *J. Chem. Phys.* **2015**, *143*, 054107.

(56) Bühl, M.; Kabrede, H. Geometries of transition-metal complexes from density-functional theory. *J. Chem. Theory Comput.* **2006**, *2*, 1282–1290.

(57) Goerigk, L.; Hansen, A.; Bauer, C.; Ehrlich, S.; Najibi, A.; Grimme, S. A look at the density functional theory zoo with the advanced GMTKN55 database for general main group thermochemistry, kinetics and noncovalent interactions. *Phys. Chem. Chem. Phys.* **2017**, *19*, 32184–32215.

(58) Altun, A.; Riplinger, C.; Neese, F.; Bistoni, G. Exploring the Accuracy Limits of PNO-Based Local Coupled-Cluster Calculations for Transition-Metal Complexes. *J. Chem. Theory Comput.* **2023**, *19*, 2039–2047, PMID: 36917767.

(59) Werner, H.-J.; Hansen, A. Accurate Calculation of Isomerization and Conformational Energies of Larger Molecules Using Explicitly Correlated Local Coupled Cluster Methods in Molpro and ORCA. *J. Chem. Theory Comput.* **2023**, *accepted*, DOI: 10.1021/acs.jctc.3c00270.